Machine Implications for Detectors and Physics

Toshiaki Tauchi

KEK,High Energy Accelerator Research Organization, 1-1 Oho, Tsukuba-shi,Ibaraki-ken, 305-0810, Japan.

Abstract. Future linear colliders are very different at many aspects because of low repetition rate (5 $\sim$ 200Hz) and high accelerating gradient (22 $\sim$ 150MeV/m). For high luminosity, the beam sizes must be squeezed in extremely small region at interaction point(IP). We briefly describe new phenomena at the IP, *i.e.* beamstrahlung process, creations of e^+e^- pairs and minijets. We also report machine implications related to the energy spread, beamstrahlung, bunch-train structure, beam polarizations and backgrounds for detectors and physics.

INTRODUCTION

From a view point of high energy experiments, the most distinct feature of e^+e^- linear colliders is a collision between very flat beams of σ_x^*/σ_y^*(aspect ratio)≈ 100 with $\sigma_y^* = 2.5 \sim 5$nm, $\sigma_x^* = 202 \sim 553$nm and the bunch length of $\sigma_z = 30 \sim 400\mu$m at $\sqrt{s}$=500GeV, where σ_y^* and σ_x^* are the vertical and horizontal beam sizes, respectively, at interaction point(IP). The beam intensity (N) is $0.4 \sim 2 \times 10^{10}e^\pm$/bunch. The another feature is a bunch-train structure. A single train consisting of $n_B = 72 \sim 2820$ bunches is accelerated by a RF pulse at a repetition rate(f_{rep}) of 5 $\sim$ 200Hz. The bunch separation ranges from 0.67 to 337 nsec depending on the width and frequency of the RF pulse.

In general, a luminosity of e^+e^- linear colliders is given by a following equation,

$$L = \frac{N^2 f}{4\pi\sigma_x^*\sigma_y^*} H_D \tag{1}$$

where f is a number of collisions in a second, *i.e.* $f = f_{rep} \times n_B = 7200 \sim 30800$, and H_D is an enhanced factor for shrinking the beam sizes by focussing forces between e^+ and e^- beams during collisions, so called pinch effect, which ranges from 1.38 to 2.3 . Higher luminosity can be obtained by increasing f and/or N. Actually, the bunch-train structure was one of consequences from the maximization of f. However, there is a limitation in a product of fN since an electric power is proportional to fN at a given beam energy. Setting bounds to the power, the fN

becomes a constant. Although Eq. (1) has another N, it is also restricted by a beam-beam force which is proportional to

$$k = \frac{N}{\sigma_x^* + \sigma_y^*} = \frac{N}{\sigma_x^*}\frac{1}{1+\frac{\sigma_y^*}{\sigma_x^*}} \approx \frac{N}{\sigma_x^*}, \tag{2}$$

as described in subsequent section. The beam-beam force induces synchrotron radiations, so called beamstrahlung, and poses undesirable problems such as energy loss, energy spread and creation of low energy e^+e^- pairs etc. . Therefore, k must be bounded. For the constant power (fN) and beam-beam force (k), the luminosity becomes to

$$L \propto \Big(\frac{1}{\sigma_x^*} + \frac{1}{\sigma_y^*}\Big)H_D = \frac{1}{\sigma_y^*}\Big(1 + \frac{\sigma_y^*}{\sigma_x^*}\Big)H_D \approx \frac{1}{\sigma_y^*}H_D \tag{3}$$

In the Eqs. (2) and (3), the last approximations are given by the flat beam. As clearly seen in the equations and H_D dose not strongly depend on the beam parameters at usual cases [1], only possibility to increase the luminosity is to make σ_y^* smaller as possible as we can [2]. However, there is a minimum of σ_y^* governed by synchrotron radiations at the final focus quadrupole magnets. The radiations generate uncontrollable energy spread to disturb the focussing strength. As the consequence, the beam spot increases in size. The focus limit depends on only the beam (invariant) emittance of $\gamma\epsilon_y$, *i.e.* $\sigma_y^* \geq 3 \times 10^{-4}(\gamma\epsilon)^{5/7}$(m) which is so called Oide-limit [3]. The actual beam sizes, which are still larger than the Oide limits, have been obtained by optimizations with other parameters.

BEAMSTRAHLUNG PROCESS

When two beams cross at IP with very small spot sizes and high intensities, they could be bent each other by a strong magnetic field accompanying the colliding beam. Thus, they must emit synchrotron radiations during collisions. This process is called as beamstrahlung specifically in e^+e^- linear colliders at TeV energies.

First, a simple case of round beams is considered for the clear description of beamstrahlung process. The magnetic field strength(H) can be calculated to be $H = 2Neb/LR^2$ (Ampere's law) at a position with an impact parameter of b for a round beam with the radius of R and the length of L as shown in Fig. 1, where N is the beam intensity and e is an electric charge. Assuming typical values of $N = 0.7 \times 10^{10}$, $b \sim R(\approx \sigma_y^*) = 3$nm, $L(\approx 2\sigma_z) = 200\mu$m, the field strength amounts to $H = 10^5$T.

$$\Delta b' \equiv \frac{\Delta b}{b} = \frac{2Nr_e}{\gamma R}\frac{b}{R} \tag{4}$$

Deflection angle ($\Delta b'$) due to the Lorentz force is estimated to be 0.03 radian by Eq. 4, where $r_e \equiv \alpha/m_e$ is the classical electron radius and $\gamma \equiv E_o/m_e$. Corresponding bending radius ($\rho = L/\Delta b'$) becomes $\rho = 1$ cm, which is too small for high energy electrons and positrons of $E_o = 250$GeV.

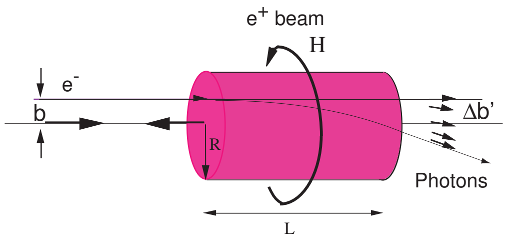

FIGURE 1. Beamstrahlung process for round beams, where an electron with a impact parameter(b) is bent by a magnetic field(H) accompanying positron beam.

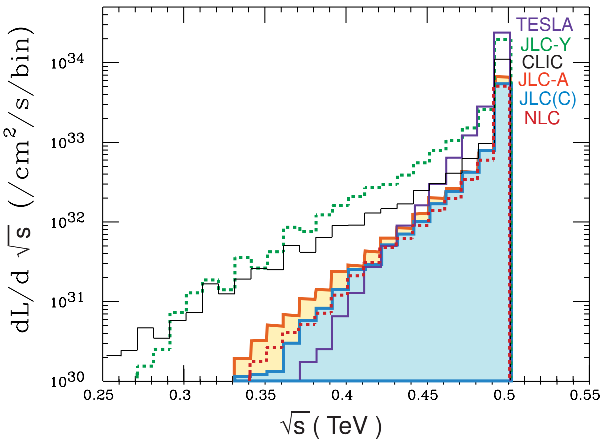

FIGURE 2. Luminosities as a function of center-of-mass energy ($\sqrt{s}$), simulated by CAIN, for TESLA, JLC-Y, CLIC, JLC-A, JLC(C) and NLC in order of peak luminosities.

For the flat beams, the magnetic field can be expressed by $H = 2Ne/L\sigma_x^*$ in a limit of $\sigma_y^*/\sigma_x^* \ll 1$. Then, the deflection angles are estimated to be

$$\Delta x'(y') = \theta_o \frac{x(y)}{\sigma_{x(y)}^*} \equiv D_{x(y)} \frac{x(y)}{\sigma_z} \tag{5}$$

$$\theta_o \equiv \frac{2Nr_e}{\gamma} \frac{1}{\sigma_x^* \sigma_y^*} \sim \Delta b' \frac{R}{\sigma_x^*} \sim \frac{\Delta b'}{100}, \quad D_{x(y)} \equiv \theta_o \frac{\sigma_z}{\sigma_{x(y)}^*}$$

with σ_x^* =300nm and $\sigma_y^* = R$, where the disruption parameter ($D_{x(y)}$) can be approximated to be σ_z/(focal length) for a thin lens approximation. So, they are numerically calculated to be $\Delta x' \sim \Delta y' \sim \theta_o \sim 300\mu$rad and the bending radius and critical energy are $\rho \approx 1$m and $U_c = 2.2 \times 10^{-6} E_o^3/\rho \sim 34$GeV, respectively. As expected, their magnitudes can be reduced by a factor of $\sigma_y^*/\sigma_x^* \approx 1/100$ compared with those of round beams. Energy loss can be also estimated to be $E_{loss} = 1.4 \times 10^{-5} E_o^4 L/\rho^2 = 11$GeV during collisions by the beamstrahlung process, therefore, $\delta_{BS} \equiv E_{loss}/E_o = 4.4\%$.

In reality, the beamstrahlung process is not so simple, for instant, the beam sizes are not constant during collisions and the magnetic field strength is a strong function of positions and time too. Thus, the beam-beam interaction is usually simulated in details by Monte Carlo programs such as ABEL [4], CAIN [5] and Guinea-Pig [6], in order to obtain the energy, angular and luminosity distributions. Figure 2 shows the luminosity distributions for proposed machines,*i.e.* TESLA, JLC, CLIC and NLC, as a function of center-of-mass energy by CAIN. All the machines have a sharp peak, where the luminosity fraction exceeds more than 70% within 98% of the nominal center-of-mass energy ($\sqrt{s_o} = 500$GeV), with tails decreasing exponentially in low energy region. Generally, comparing with initial

TABLE 1. Parameters of TESLA, NLC, CLIC, JLC-A,-Y, JLC(C) at $\sqrt{s_o} = 2E_o$=500GeV.

Parameter	unit	TESLA	NLC	CLIC	JLC-A	JLC-Y	JLC(C)
RF frequency	GHz	1.3	11.4	30	11.4	11.4	5.7
Luminosity(L)	$10^{33}/cm^2/sec$	30	7.1	14	8.8	26	7.2
L/bunch	μb^{-1}	2.1	0.62	0.46	0.63	0.92	1
H_D		2.3	1.4	1.8	1.4	1.5	1.7
$L(\sqrt{s}/\sqrt{s_o}$ >0.98)	(L/L_o)%	82	77	76	77	70	74
Energy spread	(full width)%	0.1	1		1	1	
Repetition	Hz	5	120	200	150	150	100
Beam intensity	10^{10}/bunch	2	0.95	0.4	0.75	0.7	1.1
No. of bunches	n_B/pulse	2820	95	154	95	190	72
	within 50μsec	148	95	154	95	190	72
No. of collisions	f/sec	14100	11400	30800	14250	28500	7200
Bunch separation	nsec	337	2.8	0.67	2.8	1.4	2.8
Beam power	MW/beam	11.3	4.5	4.9	4.3	8	3.1
Beam size at IP	(σ_y^*) nm	5	4.9	2.5	3.2	2.9	4.3
	(σ_x^*) nm	553	330	202	286	222	318
O ide limit	(min.σ_y^*) nm	1.3	3	0.95	2.1	1.6	1.8
Bunch length	(σ_z) μm	400	120	30	90	80	200
Diagonal angle	(σ_x^*/σ_z) mrad	1.4	2.8	6.7	3.2	2.8	1.6
Crossing angle	mrad	0	20	10	8	8	8
Disruption	D_x	0.3	0.12	0.03	0.094	0.13	0.25
	D_y	33	7.9	2.7	7.6	10	18
a ngle	θ_o mrad	0.41	0.33	0.2	0.3	0.36	0.4
Average Upsilon	$(\Upsilon_{ave} \equiv 0.67U_c/E_o)$	0.04	0.11	0.30	0.13	0.18	0.078
BS energy loss	(δ_{BS}) %	2.8	3.7	4.4	4.4	6.7	4.1
No. of BS photons	N_γ/e	1.6	1.1	0.7	1.1	1.3	1.5

state radiations(ISR), this beamstrahlung peaks are smaller, while the ISR case has longer tails at lower energies.

Major machine parameters are listed in Table 1. All the machines successfully can control the beamstrahlung process , *i.e.* $\delta_{BS} \leq$ several %, with sufficient high luminosities.

ENERGY SPREAD AND BEAMSTRAHLUNG EFFECTS

At linear colliders the energy spread is usually governed by wake fields during acceleration in the main linac, while it is determined by synchrotron radiations in the ring at conventional circular colliders. Distribution of the spread is not Gaussian but having two peaks as shown in Fig.3, although the detailed distribution is not well predicted. The full width(FWHM) ranges from 0.1 to 1% as listed in Tab. 1. Toponium production is the most sensitive process to the energy spread. The effects have been studied in details [7]. The results are shown in Fig. 3 and 4, where a peak corresponds to a 1S toponium state. Two extreme distributions with two

Gaussian peaks and flat, are also plotted in Fig. 3. When the full width is larger than 0.4%, the distribution must be experimentally determined within the energy spread for precise measurements on top-quark mass and QCD constant of α_s etc. (O(< 1%)). The beamstrahlung effect is shown in Fig. 4 together with the ISR one. Their major effect is to reduce effective luminosities.

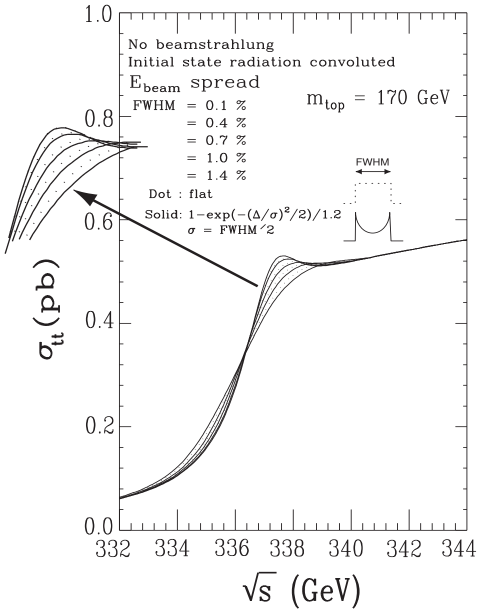

FIGURE 3. Cross section of top quark pair production as a function of $\sqrt{s}$ with no beamstrahlung, where the top quark mass is m_{top} =170GeV. Various curves correspond to cases with energy spread (FWHM) of 0.1, 0.4, 0.7, 1.0 and 1.4%. Dotted and solid curves assume the flat and double peak distributions, respectively, as shown in the figure.

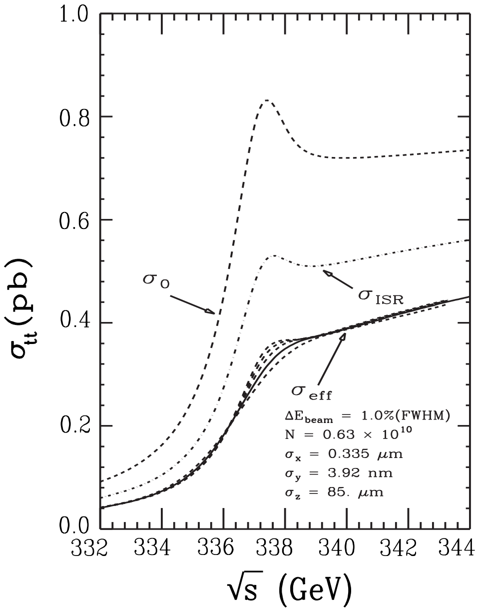

FIGURE 4. Cross section of top quark pair production as a function of $\sqrt{s}$ with m_{top} =170GeV and the energy spread of 1%, where σ_o has no beamstrahlung and no initial state radiation(ISR) and σ_{ISR} takes account of only the ISR, and σ_{eff} includes all the effects. The energy spread dependence is also plotted for σ_{eff}.

Higgs production is also sensitive to the energy spread since the natural width(Γ_{higgs}) is an order of MeV for m_{higgs} =120GeV. For the energy spreads of $\Delta E/E_o = \pm 0.1$ and $\pm 0.5\%$, Fig. 5 shows missing mass distributions reconstructed by $\mu^+\mu^-$ pairs in the process of $e^+e^- \to Zh$ and $Z \to \mu^+\mu^-$ at $\sqrt{s}$ =250GeV [8]. The smaller width enhances more peak as expected for better determination of higgs mass in principle, while tails are same in high mass region. The tails are apparently made by two effects of beamstrahlung(BS)and initial state radiation, which may be recovered into the peak by kinematical fitting [9]. Even with the nominal energy spread($\Delta E/E_o = \pm 0.5\%$) and the tails, higgs signals are clearly visible in an existence of background process $e^+e^- \to ZZ$ as shown in Fig.6. The beamstrahlung effect is the same as the toponium case.

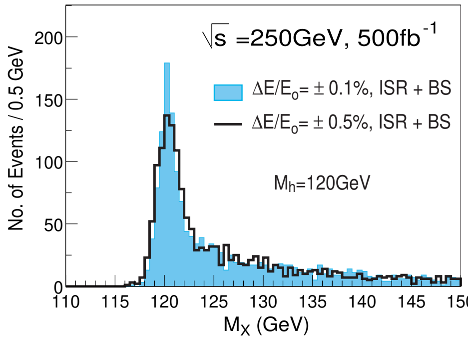

FIGURE 5. Missing mass distributions with various energy spreads in the process of $e^+e^- \rightarrow Zh$ and $Z \rightarrow \mu^+\mu^-$, which has been simulated with the JLC detector at $\sqrt{s_o}$ =250GeV and the integrated luminosity is 500 fb^{-1}, where m_{higgs} =120GeV and the ISR and beamstrahlung (BS) were included.

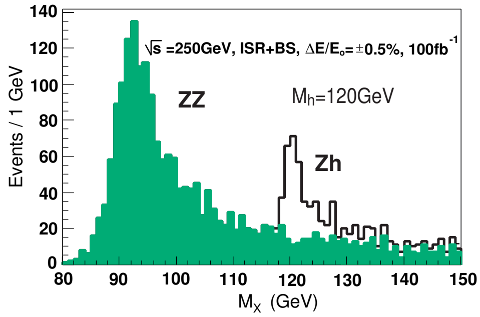

FIGURE 6. Missing mass distributions with the nominal energy spread ($\pm$0.5%) for the same process as left figure, where the major background process of $e^+e^- \rightarrow ZZ$ is also plotted both for the integrated luminosity of 100 fb^{-1}.

POLARIZED BEAMS

Polarized beams, at least for e^- beam, must be available right from the start with high polarization at linear colliders. The polarization is essential in precise measurements, especially on SUSY particles to disentangle weak mixings of neutralinos and charginos($\tilde{\chi}^{o,\pm}$), on W^+W^- pairs to probe anomalous couplings and on Giga-Z , as well as suppression of standard model backgrounds against new physics.

The most promising polarized electron source must have a superlattice structure, which is less suffered by surface charge limit(SCL), because of the large energy-gap (margin) between the conduction band and vacuum level for the high intensity necessary at linear colliders [10,11]. One candidate is a GaAs-GaAsP strained-layer superlattice which has been investigated by JLC-PES collaboration. The experimental results of polarization, quantum efficiency and multi-bunch structure are shown in Fig. 7 and 8, respectively [12,13]. Maximum polarization was obtained to be 81% with 0.3% quantum efficiency at laser wavelength of 773nm. Figure 8 shows multi-bunch beam profiles with 3nsec spacing for various laser energies. The maximum intensity was estimated to be 0.6×10^{10}/bunch and the result gives no indication of the SCL phenomenon as expected, while the present intensity was limited by space charge effect in an output cavity.

Polarized positron beam can be provided by e^+e^- pairs created in collisions between polarized photons and a metal target such as tungsten and titanium. Two methods have been considered for the polarized photons. One is to use an extracted beam ($E >$ 150GeV) passing through a wiggler as TESLA positron source. Another method employs a backward Compton scattering between circular polarized CO_2 laser ($\lambda = 10.6\mu$m, 0.35J/bunch) and E=5.8GeV electron beam(5×10^{10}/bunch), where both are multi-bunch beams(95bunches/train) [14]. With an array of 50

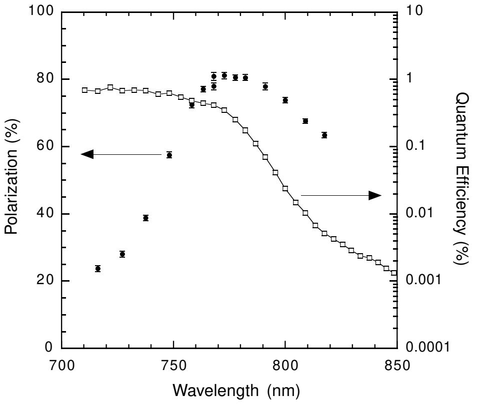

FIGURE 7. Polarization and quantum efficiency as a function of laser wavelength, measured for GaAs-GaAsP strained-layer superlattice.

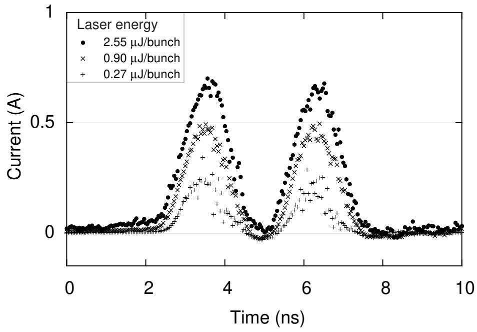

FIGURE 8. Sub-nanosecond bunches measured for GaAs-GaAsP strained-layer superlattice.

CO_2 lasers, a positron beam is expected to be produced with the intensity of 0.79×10^{10}/bunch and polarization of $\sim 60\%$.

BACKGROUNDS AND IP LAYOUT

Beam delivery system (BDS) downstream of the main linac is a machine-detector interface for clean, stable and efficient e^+e^- collisions with high luminosity. In general, the BDS consists of collimation, final focus systems, interaction region (IR) and beam extraction line.

Primary goal of the collimation is to eliminate particles at the beam halo before they cause intolerable backgrounds at a detector, that is, they and their emitting synchrotron radiations hit the vacuum pipe and the final focus magnets near the detector. Typical collimation depth is $(6 \sim 8)\sigma_x \times (35 \sim 40)\sigma_y$ for them never to hit. The halo intensity has been recently thought to be 10^{-3} as experienced at SLD/SLC [15], while the simple calculation shows 10^{-7} based on residual gas scatterings at vacuum pressure of 10^{-8} torr. Since muons are created in an electromagnetic interaction at a rate of $N_\mu = 2.3 \cdot 10^{-4} \cdot E_e/250$GeV for $E_\mu >$5GeV, the collimation yields muons at the rate of 10^3 or 10^{-1}/bunch. Simulations show that several % of the muons hit the detector without any shield and the tolerable hit rate of 1 muon/train or during a readout time of 50μsec can be realized by muon spoilers and attenuators(cylinders).

At IP, a lot of low energy e^+e^- pairs are created in three processes of $\gamma_{bs}\gamma_{bs} \to e^+e^-$(BW), $\gamma_{bs}e^{+(-)} \to e^+e^-e^{+(-)}$(BH) and $e^+e^- \to e^+e^-e^+e^-$(LL), where γ_{bs} is a beamstrahlung photon, as shown in Fig.9. The cross sections are orders of $10^{-27}, 10^{-25}$ and 10^{-26}cm^2 for BW,BH and LL, respectively. Since the luminosity and the number of γ_{bs} are orders of magnitude of 1μb^{-1}/bunch and 1/electron, respectively, as listed in Tab. 1, the total number of pairs must be an or-

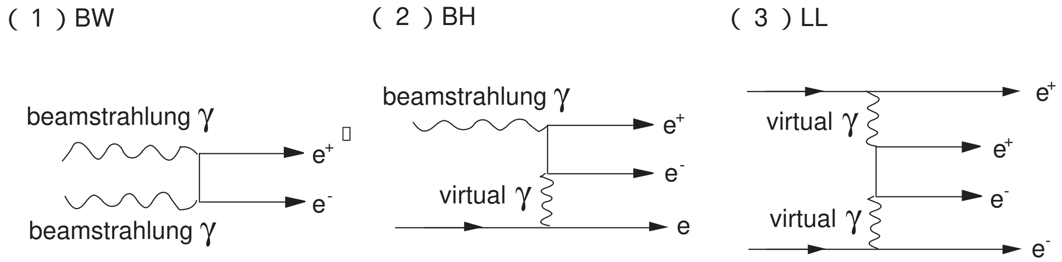

FIGURE 9. Incoherent $e^{\pm}$ pair creation processes; (1) Breit-Wheeler (BW), (2) Bethe-Heitler (BH) and (3) Landau-Lifshit (LL) processes.

der of 10^5/bunch. Actually the CAIN simulation shows that they are created at rates of $1.9 \cdot 10^3$,$2.2 \cdot 10^5$ and $4.5 \cdot 10^4$/bunch for BW,BH and LL, respectively, at JLC-A. Although their inherent scattering angles are very small($\approx m_e/E_e$), they must be strongly affected by the magnetic field accompanying colliding beam as discussed in the previous section. Especially particles with the same charge as the colliding beam are bent in large angular region, while the other charged particles oscillate around the beam axis. Their angles have been calculated to be $\theta_x \approx \theta_y \approx \sqrt{\log(4\sqrt{3}D_x/\epsilon)/\sqrt{3}\epsilon D_x} \cdot \theta_o$ for $D_x/\epsilon \geq 1$ with $\epsilon \equiv E_e/E_o$ [1], typically $\theta_{x,y} \approx 100$mrad for E_e =100MeV and E_o=250GeV.

When particles acquire transverse momenta (p_t) to move along helical orbits in the detector magnetic field (B), some of them produce background hits, especially in the vertex detector (VTX) close to the beam axis. At $B = 3$Tesla, particles with $p_t \geq 11.2(6.75)$ GeV can pass through a cylindrical surface of $r = 2.5(1.5)$cm which may correspond to the minimum radius of the VTX. Such particles are so many that the background rate is usually expressed by their density at the surface. Track densities ($|\cos\theta| \leq 0.95$) are listed for proposed machines in Tab.2. For JLC-A and -Y, hit densities are also listed in this table, *i.e.* specified by JIM:hits, which were estimated with the JLC detector by a Monte Carlo simulation (JIM). Comparing with the track and hit densities, a track produces about 10 background hits on average. So, typical hit densities within $|\cos\theta| \leq 0.95$ are expected to be $0.5 \sim 1$ and $4 \sim 10/\text{mm}^2$ per train or 50μsec at r=2.5 and 1.5cm, respectively, assuming B =3Tesla. For the reduction of hit densities, the higher B field and smaller angular acceptance are preferred and must be optimized, since the tolerance is a few hits/mm^2 by a track finder. Such high hit rates require a fine segmented detector, it i.e. pixel devices (CCD and APS).

Most of the particles hit the final focus magnets located at $\ell^* = 2 \sim 4.3$m from the IP. Major secondary backgrounds are photons and neutrons back-scattered from the electromagnetic showers, where the typical energies are 500KeV of a peak from positron annihilation and a few MeV from giant resonances, respectively. The

TABLE 2. Background (pairs, neutrons) estimations for TESLA, NLC, CLIC, JLC-A,-Y, JLC(C) at $\sqrt{s_o} = 2E_o$=500GeV, by CAIN.

Parameter	unit	TESLA	NLC	CLIC	JLC-A	JLC-Y	JLC(C)
No.of pairs;E>3MeV	/bunch	91976	26697	15049	23385	40987	51033
Total pair energy	TeV/bunch	202	98	88	94	194	161
Neutrons(0.1n/GeV)	10^4n/bunch	2	1	1	1	2	2
n at VTX	$10^7/cm^2$/year	< 5	400(1TeV)		7		
Average pair energy	GeV	2.2	3.7	5.9	4	4.7	3.1
Photons ($4\gamma/e$)	10^4/bunch	37	11	6	9	16	20
Pairs							
$\lvert\cos\theta\rvert < 0.95, p_t > 11.2$MeV	/bunch	34	15	6	7	12	17
tracks at r=2.5cm,B=3T	/bunch/cm^2	0.2	0.1	0.04	0.05	0.08	0.1
JIM:hits at r=2.5cm,B=3T	/train/mm^2				0.5		
$\lvert\cos\theta\rvert < 0.95, p_t > 6.75$MeV	/bunch	118	46	93	26	93	57
tracks at r=1.5cm,B=3T	/bunch/cm^2	1.4	0.5	1.1	0.3	1.1	0.7
JIM:hits at r=1.5cm,B=3T	/train/mm^2				3.6		
Beamstrahlung(BS)							
BS photons	N_γ/e	1.6	1.2	0.7	1.1	1.2	1.5
Average photon energy	GeV	4	7.9	15	8.9	11	6.7
Total power	KW	293	167	209	160	438	126
Neutrons(10^{12}n/KW)	10^{14}/sec	3	2	2	2	4	1
n at VTX	10^7/cm^2/year	28	25(1TeV)		2.5		

production rates of photons and neutrons are 4γ per particle and $1n$ per 10GeV energy deposits, respectively, on average. The estimated numbers are also listed in Tab.2. We shall also take account of photon yields from particles hitting the beam pipe and the VTX, so an optimization of these geometries is essential in order to minimize the photon generation.

Since the photons cause intolerable background hits in central tracking chambers(jet-type or TPC), a conical mask must be installed to absorb them together with a cylindrical one surrounding the final focus magnet as shown in Fig.10. The conical mask must be instrumented to be a detector for hermetic calorimetry together with the inside detectors such as luminosity monitor. The minimum angle of the calorimetry, so called veto angle(θ_{veto}), is very important to discriminate new signals from two-photon processes. For instant, stau($\tilde{\tau}$) pair production can be well selected from dominant background of $e^+e^-\tau^+\tau^-$ if θ_{veto} is 50mrad as demonstrated in Fig. 11 [16]. Usually, the veto angle is determined by the maximum radius of the helical orbits and the location of the luminosity monitor which are directly related to B and ℓ^*, respectively.

Neutrons have two major effects. First, they produce background hits in the same way as photons. Total number of neutrons is about $1 \sim 2 \cdot 10^4$/bunch at most as listed in Tab.2. The above mask system is also effective for the neutron shield. However, it may require additional shield between the detector and the mask system, whose material must have hydrogens, such as polyethylene, doped with borons for neutron absorption. The background hit rate is expected to be similar to that of the photons. Second effect is a radiation damage on the VTX. The neutron flux has been estimated by TESLA, NLC and JLC groups and the results are also listed in Tab.2. They are all sufficiently below the tolerance of $1.5 \cdot 10^{10} n/\mathrm{cm}^2$ assuming the VTX is a CCD type [17].

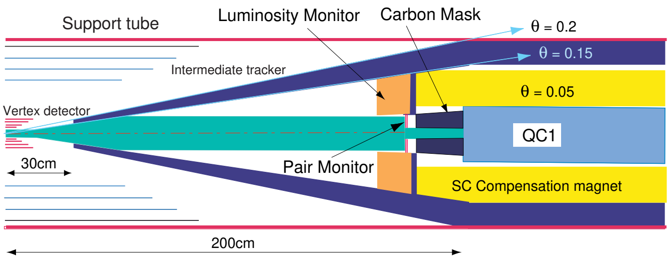

FIGURE 10. JLC interaction region optimized at B=2 Tesla, where the final focus magnet(QC1) is located $\ell^* =$ 2m from the IP and the veto angle is 50mrad. The masks are made of tungsten.

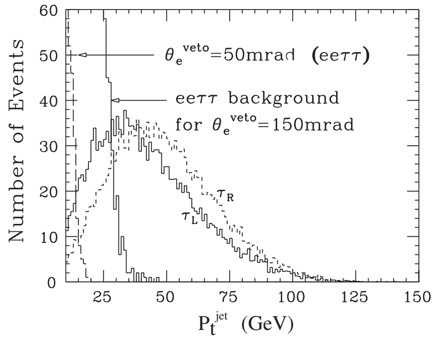

FIGURE 11. Transverse momentum distribution of jets from stau decays ($\tilde{\tau} \rightarrow \tau\tilde{\chi}_1^o$), $m_{\tilde{\chi}_1^o}$=100GeV, $m_{\tilde{\tau}}$=150GeV at $\sqrt{s}$=500GeV.

More neutrons are actually generated at the beam extraction line and dumps both for $e^{\pm}$ beams and beamstrahlung photons whose total powers are $3 \sim 11$MW and $126 \sim 438$KW, respectively. Since neutrons are generated at a rate of $10^{12} n/\mathrm{KW}$, an energy loss(E_{loss}) at the extraction line must be sufficiently small as $E_{loss}/E_o \ll 1\%$ and the dumps must be water tanks doped with borons. Amount of E_{loss} seems to be balanced with diagnosis of beam properties, *i.e.* capabilities of the energy spread and polarizations at the extraction line.

In addition to the e^+e^- pairs, there are jets productions in two photon process, so called minijets [18], of $\gamma\gamma \rightarrow q\bar{q}$ where γ is a virtual or beamstrahlung photon. Although, the cross section strongly depends on a model of hadronic structure of photon with large uncertainty, it has been estimated to an order of 0.1μb. Since the luminosity per bunch is about $1\mu\mathrm{b}^{-1}$, the minijets may cause an event overlap at probability of O(10%) assuming perfect bunch identification in each event. Figure 12 shows the event overlap effects on the reconstruction of Higgs mass in $e^+e^- \rightarrow \nu\bar{\nu}h$ [19]. As clearly seen, even a minijet-event overlap significantly degrades the mass distribution. Although the degradation can be partially recovered by limiting a detector acceptance because of the two photon process nature, a good time resolution must be required for detectors in order to identify a specific bunch. The capability of good time-stumps($<$ 1nsec) is essential especially for short bunch spacing machines of NLC, JLC and CLIC.

CONCLUSION

During collisions at linear colliders, a large fraction of beams may loose a significant amount of energies by radiations by beam-beam force which is called as

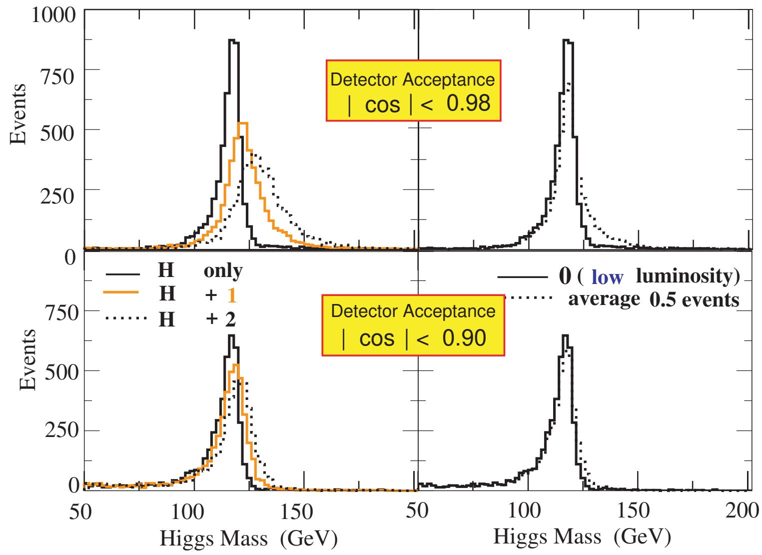

FIGURE 12. Distributions of reconstructed Higgs mass in the process of $e^+e^- \to \nu\bar{\nu}h$ for angular regions of $|\cos\theta|$ <0.98(top) and 0.90(bottom); left with 1, 2 and 3 minijet-events and right with 0.5 ones on average.

beamstrahlung. With a constant electric power for the linear collider operation and a bound for the beam-beam force, the luminosity shall be maximized by making flat beams as much as possible. So the beamstrahlung process is under control in keeping high luminosity.

Major effect of the beamstrahlung has been found to reduce the effective luminosity in the same way as the initial state radiation, especially for toponium and higgs studies. If the energy spread of more than 0.4%, the energy distribution within the spread must be measured for toponium physics. Beam polarizations certainly strengthen the capability of precise measurements. We expect more than 80% and 60% polarizations for electron and positron beams, respectively.

The beams are collimated far up the stream in order to be enough for the beam line aperture with no scattering of emitted synchrotron radiation and themselves, while the detector can be shield from generated muons by muon spoilers and attenuators. The creation and deflection of $e^{\pm}$ pairs can be simulated in details. Flux of the primary particles requires a pixel device for the vertex detector whose minimum radius can be minimized by increasing the detector magnetic field. A veto angle of $\theta_{veto} \leq$ 50mrad is possible, which might be essential for SUSY signals. The secondaries of photons and neutrons can be absorbed by masks. In order to resolve the event overlap with minijets, the detector must have a good time resolution. Thus, all the backgrounds can be reliably estimated and under control.

Therefore, all machines and detectors are close to be optimized and ready to experiments.

REFERENCES

1. K. Yokoya and P. Chen, “Beam-beam phenomena in linear colliders”, lecture at 1990 US-CERN School on Particle Accelerators, Nov.7-14, 1990, Hilton Head Island, So. Carolina, USA, Lecture Notes in Physics 400. *Frontiers of Particle Beams: Intensity Limitations* , Springer Verlag, pp.415-445.
2. K. Oide, proceedings of JLC-FFIR92 (japanese), pp.195-295, KEK Proceedings 93-6, June 1993.
3. K. Oide,*Phys. Rev. Lett.* **61** , 1713(1988).
4. K. Yokoya, KEK-Report 85-9 (1985); also Nucl. Instr. and Meth. **A251** (1986), 1.
5. P. Chen, G. Horton-Smith, T. Ohgaki, A.W. Weidemenn, K. Yokoya, Nucl. Instr. and Meth. **A355** (1995) 107. The latest version can be obtained from a web site of http://www-acc-theory.kek.jp/members/cain/default.html.
6. D. Schulte, “Beam-beam simulations with GUINEA-PIG,” CERN-PS-99-014. The latest version can be obtained from a web site of http://www-sldnt.slac.stanford.edu/nlc/programs/guinea_pig/gp_index.html.
7. K. Fujii, T. Matsui and Y. Sumino, *Phys. Rev. D* **50** , 4341(1994).
8. A. Miyamoto, talk on ”Performance of JLC tracking system” at this workshop, in these proceedings.
9. A. Juste, talk on ”Higgs Mass Determination from Direct Reconstruction at a Linear Collider” in proceedings of the International Workshop on Linear Colliders (LCWS99), Sitges, Barcelona, Spain, April 28- May 5, 1999, also in FERMILAB-Conf-99/352, December 1999.
10. T. Nakanishi et al., *AIP Conf. Proc.* **421** ,300(1998).
11. K. Togawa et al.,*Nucl. Instrum. Methods A* **414** , 431(1998).
12. K. Togawa et al.,*Nucl. Instrum. Methods A* **455** , 118(2000).
13. K. Togawa et al., International Workshop on Polarized Electron Sources and Polarimeters (PES2000), October 12-14, 2000, Nagoya,Japan, to be published in SPIN2000 Proceedings (AIP. Conf. Proc.)
14. T. Omori, talk on ”A Polarized Positron Beam for Linear Colliders” in proceedings of The 1st ACFA Workshop on Physics and Detector at the Linear Collider,November 26 - 27, 1998 at Tsinghua University, Beijing, China, KEK Proceedings 99-12, September 1999.
15. P. Tenenbaum, talk on ”NLC Post Linac Collimation”, proceedings of VIII International Workshop on Linear Colliders (LC99),October 21-26, 1999,Frascati (Rome) Italy.
16. M. Nojiri, K. Fujii, T. Tsukamoto, *Phys. Rev. D* **54** , 6756(1996).
17. A. Miyamoto, talk on ”New Estimate of Neutron Background in the JLC Detector” in proceedings of LC99.
18. Most recent review can be found in a paper entitled ”Hadronic cross-sections in $\gamma\gamma$ processes and the next linear Collider” by R.M. Godbole and G. Pancheri, LNF-00/024(P),hep-ph/0010104, October 11, 2000, and references therein.
19. S. Yamashita and J. Kanzaki, talk on ”Effects of Beam-beam Interaction, Event-Overlap in Higgs Measurements” in proceedings of LCWS99.